Electronic supplementary Information

Application of MXene for Remediation of Low-Level Radioactive Aqueous Solutions Contaminated with ^{133}Ba and ^{137}Cs

Vipul Vilas Kusumkar[a ‡], Shalu Atri[b*‡], Süleyman İnan[c], Maros Gregor[d], Tomas Roch[d], Hryhorii Makarov[d], Maria Caplovicova[e], Michal Galambos[a], Eva Viglasova[a], Gustav Plesch[b], Olivier Monfort[b*]

[a]*Department of Nuclear Chemistry, Faculty of Natural Sciences, Comenius University Bratislava, Ilkovicova 6, Mlynska dolina, 842 15 Bratislava, Slovakia*

[b]*Department of Inorganic Chemistry, Faculty of Natural Sciences, Comenius University Bratislava, Ilkovicova 6, Mlynska dolina, 842 15 Bratislava, Slovakia, Email: monfort1@uniba.sk, shalu1@uniba.sk*

[c]*Ege University Institute of Nuclear Sciences, 35100 Bornova-İzmir, Türkiye*

[d]*Department of Experimental Physics, Faculty of Mathematics, Physics and Informatics, Comenius University in Bratislava, Mlynska dolina F2, 842 48 Bratislava, Slovakia*

[e]*STU Center for Nanodiagnostics, Faculty of Materials Science and Technology in Trnava, Slovak University of Technology in Bratislava, Slovakia, Vazovova 5, 812 43 Bratslava, Slovakia*

‡ These authors contrbuted equially to the work.

** Corresponding authors: shalu1@uniba.sk (SA) and monfort1@uniba.sk (OM)*

CRediT Statement

Vipul Vilas Kusumkar: Investigation - Writing: original draft. **Shalu Atri**: Conceptualization - Investigation - Methodology - Writing: original draft - Writing: review & editing - Funding acquisition. **Suleyman Inan**: Investigation - Visualization - Writing: original draft. **Maros Gregor**: Investigation - Funding acquisition. **Tomas Roch**: Investigation. **Hryhorii Makarov**: Investigation. **Maria Caplovicova**: Investigation. **Michal Galambos**: Supervision. **Eva Viglasova**: Supervision - Methodology. **Gustav Plesch**: Supervision. **Olivier Monfort:** Conceptualization - Supervision - Writing: original draft - Writing: review & editing - Funding acquisition.

Preparation of MXene:

Ti_3AlC_2 (≥ 90%) was purchased from Sigma-Aldrich (Germany), NH_4F (97.0%) CentralChem (Slovakia). $Ti_3C_2T_x$ was prepared by acid-salt etching route using the following route: firstly 2.96 g of NH_4F was dispersed in 20 ml of concentrated HCl solution on ultrasonication for 30 minutes and then 500 mg of Ti_3AlC_2 powder was slowly added to this solution and kept on magnetic stirrer for 48 hours at 25 °C. The obtained product was washed with distilled water till natural pH and then dried using vacuum-assisted filtration system, and it is referred as unwashed MXene (UW-MXene). Whereas, in the case of acid-washed MXene (AW-MXene), the obtained product was washed with 2 M HCl solution, followed by several washing steps with distilled water and isopropanol to remove the by-products and then dried at using vacuum-assisted filtration system.

Characterization of MXene:

The MXene samples were characterized *via* powder X-ray diffraction (PXRD, PANalytical X-ray diffractometer equipped with CuK_α radiation), scanning electron microscopy (SEM, Tescan Lyra III), X-ray photoelectron spectroscopy (XPS, Omicron multiprobe system equipped with hemispherical mirror analyzers and monochromatic Al K_α radiation), Brunauer Emmett-Teller technique (BET, Sorptomatic 1990 instrument), Fourier-transform infrared spectrometer (FTIR, JASCO 4600), and transmission electron microscopy (TEM, JEOL JEM ARM 200 cF).

Adsorption experiments:

Radiotracer were ^{133}Ba in the form of [^{133}Ba] $BaCl_2$ (Eurostandard CZ s.r.o., Czech Republic) with a volume activity of 2MBq/mL and ^{137}Cs in the form of [^{137}Cs] CsCl (National Centre for

Nuclear Research, Poland) with a volume activity of 55 MBq/mL. The sorption studies of ^{133}Ba and ^{137}Cs onto a AW-MXene were investigated using radioisotope indication methods. Batch experiments were conducted under aerobic conditions at room temperature, with 0.025 g of MXene mixed with 5 mL of aqueous phase in a plastic tube. The sorption parameters were evaluated by analyzing an aliquot supernatant, after centrifugation of the suspension, by a gamma spectrometer equipped with a NaI(Tl) detector. The statistical error of the measurements was less than 1%.

Equilibrium concentration (C_{eq})

$$C_{eq} = \frac{C_0 \times a}{a_0} \quad \text{(mol/L)} \qquad (1)$$

Distribution coefficient (K_d)

$$K_d = \left[\frac{a_0 - a}{a}\right] \times \frac{V}{m} \quad \text{(mL/g)} \qquad (2)$$

Sorption capacity (q)

$$q = K_d \times C_{eq} \quad \text{(mmol/g)} \qquad (3)$$

Equations were used to calculate the equilibrium concentration (C_{eq}), distribution coefficient (K_d), and sorption capacity (q) of ^{133}Ba and ^{137}Cs onto MXene. Specifically, C_0 and C_{eq} represent the initial and equilibrium concentration (in mol/L), respectively, V corresponds to the volume of aqueous phase (in mL), m is the mass of sorbent (in g), a and a_0 refer to the initial and equilibrium volume activity of the solution (in mL/s), respectively, and K_d denotes the distribution coefficient of ^{133}Ba (in mL/g).

Text S1:

The presence of two peaks in Ti 2p spectra corresponds to Ti $2p_{3/2}$ and Ti $2p_{1/2}$ peaks that arise due to spin-orbit coupling. On deconvolution of Ti 2p spectra, six peaks occur at 454.8, 455.7, 456.5, 461.1, 462.7, 463.6 eV. A difference of ~ 1.0 eV in consecutive Ti $2p_{3/2}$ peaks refers to presence of Ti as Ti-O/O/O (454.8), Ti-O/O/F (455.7) and Ti-O/F/F (456.5). The XPS spectrum of carbon shows binding of carbon with Ti and other carbon atoms. In the XPS spectrum of oxygen, splitting of peaks exhibits two types of oxygen atom bonded with titanium atoms. A shoulder occurring in the F spectra might be due to the presence of a small amount of AlF_3 as impurity or byproducts. The presence of a small amount of N is quite feasible due to the usage of excess ammonium fluoride during etching conditions.

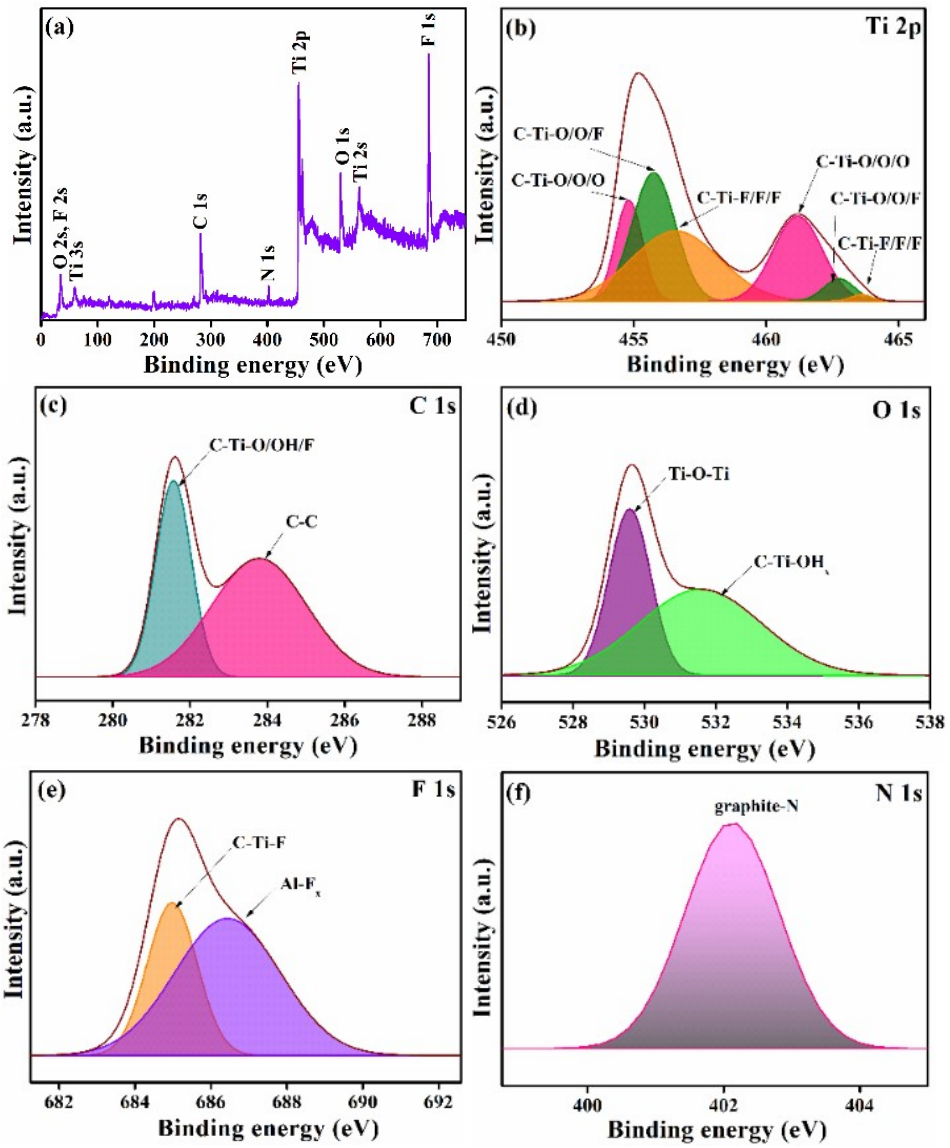

Fig. S1 The XPS (a) survey spectra for $Ti_3C_2T_x$ MXene and respective core spectra of (b) Ti 2p, (c) C 1s, (d) O 1s, (e) F 1s and (f) N 1s.

Text S2:

The linear form of the pseudo-first-order equation[1] is expressed as follows:

$$ln(q_e - q_t) = lnq_e - k_1 \times t \quad (4)$$

where q_t and q_e are the amounts of metal ions sorbed at equilibrium (mg/g) and t (min), respectively, and k_1 is the rate constant of the equation (min^{-1}). The sorption rate constant (k_1) represents the slope of the graph course drawn between $ln(q_e\text{-}q_t)$ and t.

The pseudo-second-order model has been proposed to predict the kinetic behavior of adsorption where chemical sorption is the rate control step. The linearized form of the model is expressed as follows[2,3]:

$$\frac{t}{q_t} = \frac{1}{k_2 \times q_e^2} + \left(\frac{1}{q_e}\right) \times t \quad (5)$$

where k_2 is the second-order rate constant (g/mg min), q_t and q_e (mg/g) are the amount of metal adsorbed at adsorption time t (min) and equilibrium, respectively. The parameters of pseudo-first-order and pseudo-second-order models were summarized in Table S1.

Table S1. Pseudo-first- and second-order model parameters for Ba^{2+} and Cs^{+} adsorption on MXene.

	Pseudo-First-Order			Pseudo-Second-Order		
	k_1 (1/min)	q_e (mg/g)	R^2	k_2 (g/mg min)	q_e (mg/g)	R^2
Ba^{2+}	0.011	11.40	0.954	2×10^{-3}	18.25	0.996
Cs^{+}	0.014	12.87	0.808	2×10^{-3}	18.28	0.991

The intraparticle diffusion model proposed by Weber and Morris (1963) is based on pore diffusion and can be expressed in the following linearized form[4]:

$$q_t = K_i \times t^{0.5} + C \quad (6)$$

This model assumes that the rate-limiting step in the adsorption process is the diffusion of solute molecules within the pores of the adsorbent material.[5] The linear relationship between q and t suggests that the intraparticle diffusion is the only significant mechanism controlling the adsorption process. However, in practice, adsorption usually involves multiple mechanisms, and the intraparticle diffusion model is often used in combination with other models to better describe the adsorption process. The model is defined by a plot expressing the relationship between metal uptake (q_t) and the square root of time ($t^{1/2}$). K_i is the intraparticle diffusion rate constant (mg/g $min^{0.5}$) and C value denotes the boundary layer thickness. The calculated model parameters are provided in Table S2.

Table S2. Intraparticle diffusion model parameters for Ba^{2+} and Cs^{+} sorption on MXene.

	First stage			Second stage		
	K_{id1} (mg/g $min^{0.5}$)	C	R^2	K_{id1} (mg/g $min^{0.5}$)	C	R^2
Ba^{2+}	0.496	8.05	0.894	0.054	16.20	0.549
Cs^{+}	0.850	3.87	0.842	0.012	16.96	0.274

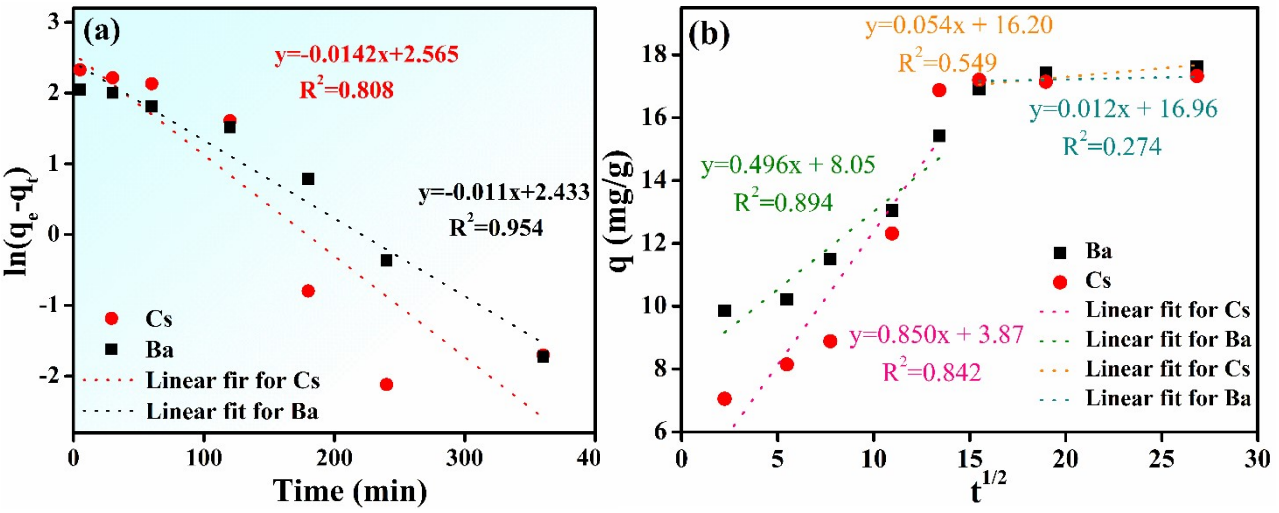
(a)
y=-0.0142x+2.565
R2=0.808
y=-0.011x+2.433
R2=0.954
Cs
Ba
Linear fir for Cs
Linear fit for Ba
ln(qe-qt)
Time (min)
(b)
y=0.054x + 16.20
R2=0.549
y=0.012x + 16.96
R2=0.274
y=0.496x + 8.05
R2=0.894
y=0.850x + 3.87
R2=0.842
Ba
Cs
Linear fit for Cs
Linear fit for Ba
Linear fit for Cs
Linear fit for Ba
q (mg/g)
t1/2

Fig. S2 (a) Pseudo first-order and **(b)** Intraparticle diffusion kinetic models of Ba^{2+} and Cs^{+} adsorption on MXene.

Table S3. Literature comparison of MXene materials in removal of heavy metal ions.

Compositions	**Ions**	**Synthesis method**	**Adsorbate conc.**	**Adsorbent conc.**	**Removal capacity**	**Ref.**
$Ti_3C_2T_x$	Cs^{+}	In-situ HF etching by using HCl+NaF	5 mg/L of Cs^{+}	1 g/L	25.4 mgg^{-1} was achieved within one minute at pH=6	6
$Ti_3C_2T_x$	Ba^{2+}, Sr^{2+}	Commercial powder	2 g/L of Ba^{2+} and Sr^{2+}	100 g/L	180 (Ba^{2+}) and 225 (Sr^{2+}) mg/g	7
$Ti_3C_2T_x$	Ba^{2+}	HF etched $Ti_3C_2T_x$	55 mg/L of Ba^{2+}	5 to 100 mg/L	9.3 mg/g	8

$Ti_3C_2T_x$ and Alk - $Ti_3C_2T_x$	Ba^{2+}	$Ti_3C_2T_x$ using HF etching methos, Alk-$Ti_3C_2T_x$- Immersing in 5% NaOH followed by washing and drying at RT/48 h	50 to 500 mg/L	0.5g/L	46.46 mg/g (three times higher than pristine $Ti_3C_2T_x$)	9
$Ti_3C_2T_x$	Cs^+	In-situ HF etching by using HCl + NH_4F	132 mg/L (Ba^{2+}) and 137 mg/L (Cs^+)	5 g/L	154.9 and 121.5 mg/g for ^{133}Ba at natural pH	This work

Text S3: The Langmuir model assumes that the adsorption is monolayer and takes place at certain homogeneous regions on the adsorbent surface. The linearized form of Langmuir equation can be written as follows[10]:

$$\frac{C_e}{q_e} = \frac{C_e}{q_m} + \left(\frac{1}{q_m \times b}\right) \quad (7)$$

where q_e is the amount of metal ion adsorbed at equilibrium (mol/g), C_e is the concentration of metal ion in the solution at equilibrium (mol/L), q_m is the monolayer adsorption capacity (mol/g) and b is the constant related to free energy of adsorption (L/g).

The Freundlich model[11] can be applied for multilayer sorption on heterogeneous surfaces. It is written in its linear form as,

$$logq_e = logK_f + \frac{1}{n} \times logC_e \quad (8)$$

where K_f is a constant related to the adsorption capacity and *1/n* is a parameter-dependent on the adsorption intensity.

The Dubinin-Radushkevich (D-R) isotherm is used to explain the adsorption process on a heterogeneous and porous surface.[12] The linear form of the D-R isotherm model is expressed in Eq. (9), where β is the coefficient related to adsorption energy (mol^2/J^2), q_m is the theoretical saturation capacity (mg/g), and ε is the Polanyi potential.[13]

$$lnq_e = lnq_m - \beta\varepsilon^2 \quad (9)$$

Table S4. Langmuir, Freundlich, and Dubinin-Radushkevich (DR) isotherms model parameters.

Isotherm parameters	Values	
	Ba^{2+}	Cs^+
Langmuir		
q_m (mg/g)	260.13	231.05
b (L/g)	1033.6	1957.7
R^2	0.193	0.153
Freundlich		

1/n	0.693	0.619
K_f	0.034	0.012
R^2	0.945	0.929
Dubinin-Radushkevich (DR)		
q (mg/g)	19.46	13.10
β $(mol/J)^2$	1×10^{-7}	7×10^{-8}
R^2	0.657	0.571

Text S4:

PXRD results revealed peak broadening and shift in peak position towards lower 2θ for AW-MXene compared to UW-MXene, which is in favor of high adsorption performance (Fig. S3). Also, AW-MXene before and after adsorption exhibited similar peak position, thus highlighting the stability of the multilayer structure (Fig. S3). FTIR spectra recorded for AW-MXene and UW-MXene after adsorption, depicted diminished bands for NH_4^+ ion, while a new band appeared at 3450 cm^{-1}, clearly showing the presence of the -OH functional group that confirmed binding of Ba^{2+} and Cs^+ ion with NH_4^+ ion (Fig. S4).

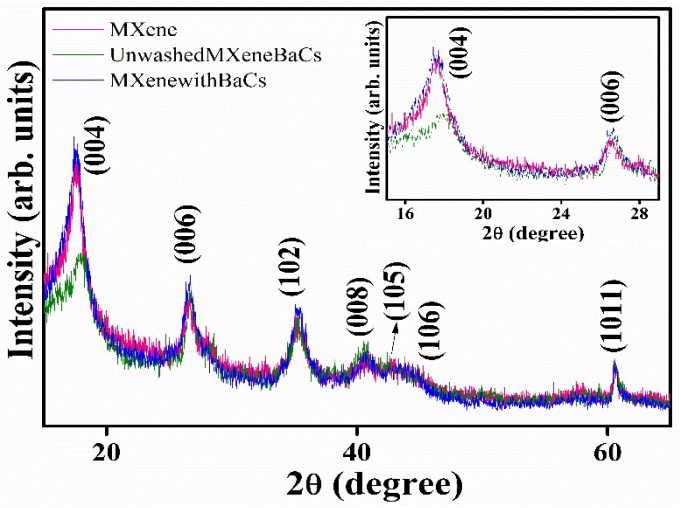

Fig. S3 Comparison of PXRD patterns for pristine MXene before adsorption, and AW-MXene and UW- MXene after adsorption of Ba^{2+} and Cs^{+} (inset shows zoomed area at lower 2θ region).

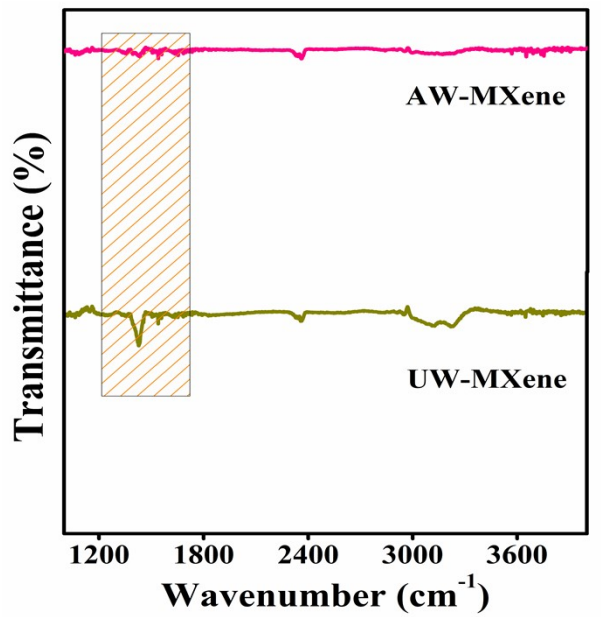

Fig. S4 FTIR spectra for AW-MXene and UW-MXene after Ba^{2+}/Cs^{+} adsorption.

Text S5:

In the XPS survey spectra of both AW-MXene and UW-MXene samples after adsorption treatment (Fig. S4), the appearance of doublet around 799.6 and 783.5 corresponds to Ba 3d, thus confirming the adsorption of Ba^{2+} ion on MXene surface. Especially, there is significant shift towards higher binding energy observed for each element in the XPS spectra of AW-MXene in comparison to UW-MXene, and that supports the high adsorption performance of AW-MXene due to utilization of its functional group in bonding with Ba^{2+} and Cs^{+} ion (Fig. S5). In addition, the changes of band ratio or even their appearance in core spectra of Ti 2p, C 1s, O 1s and F 1s suggested surface changes took place at the MXene surface, after adsorption treatment, thus suggesting functional groups at MXene surface bonded with Ba^{2+}/Cs^{+} ions during adsorption (Fig. 3 and S5).

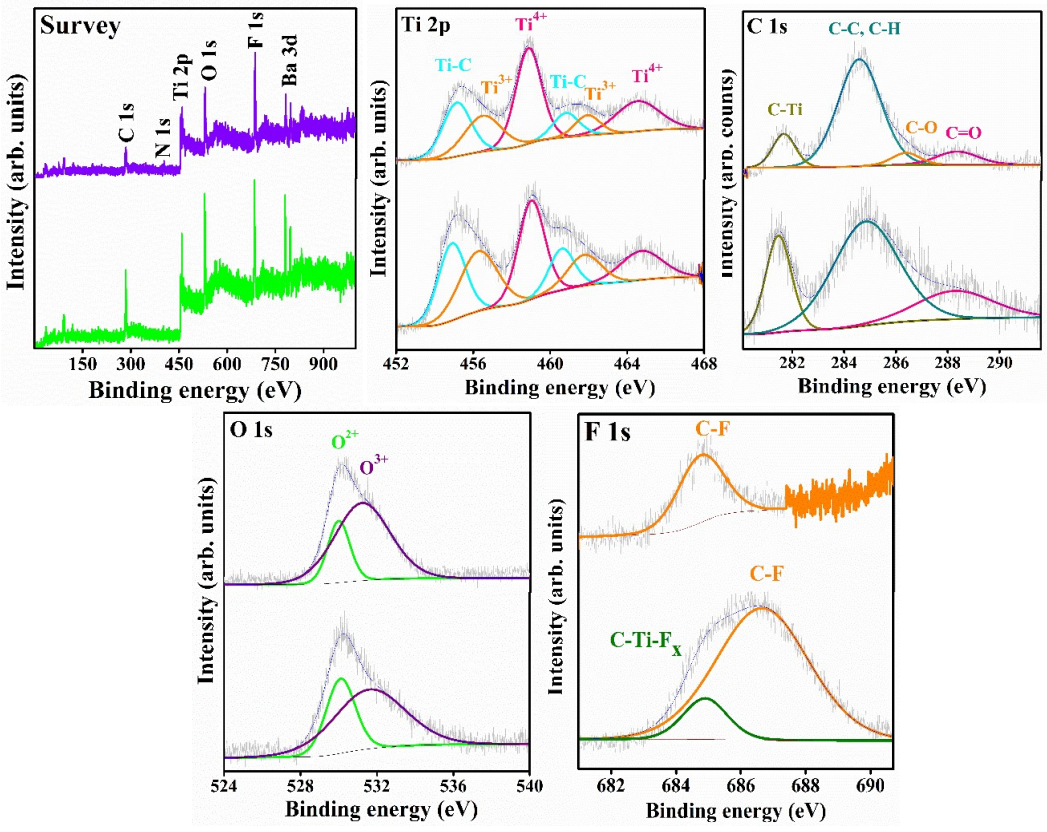

Fig. S5 XPS survey and core spectra of Ti 2p, C 1s, O 1s and F 1s of the AW-MXene and UW-MXene samples after Ba^{2+}/Cs^{+} adsorption treatment. In each spectrum, AW-MXene is at bottom and UW-MXene is at the top.

Text S6:

Selectivity coefficient (β) is used to quantify a material's affinity or preference for a particular ion. A higher selectivity coefficient indicates that the material has a stronger preference for that ion over other ions in a mixture. In other words, the material is more selective towards that ion. Therefore, a greater selectivity coefficient represents a greater degree of preference for the ion by the material and it is expressed as in Eq(10)[14,15]:

$$\beta_{1,2} = \frac{K_{d1}}{K_{d2}} \tag{10}$$

In Eq. (10), K_{d1} and K_{d2} refer to distribution coefficients of ^{133}Ba and ^{137}Cs, respectively.

Note: Having a β value greater than 2 is usually desired for achieving an effective separation.

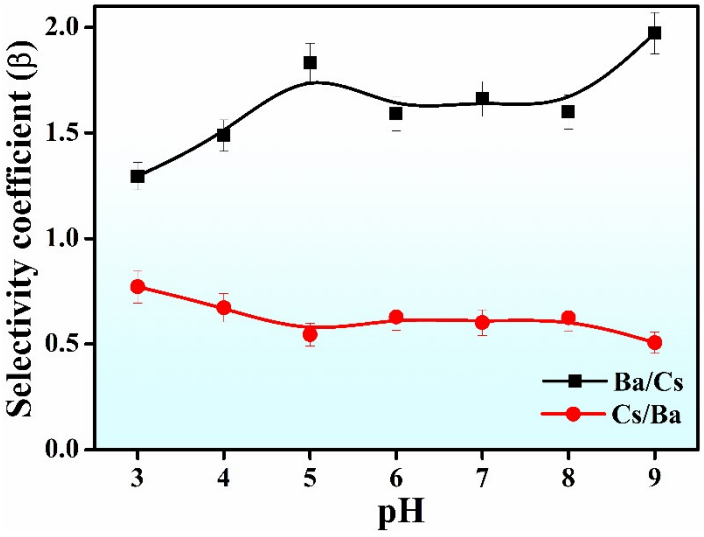

Fig. S6 The effect of pH on selectivity coefficient (β) (C_0: 0.001 mol/L, t: 3 h, m/V: 5 g/L, T: laboratory conditions).

Text S7:

The effect of singular cation (Na^+, Mg^{2+}, Co^{2+}, Ca^{2+} and K^+) on the performance of MXene for the removal of Ba^{2+} and Cs^+ radionuclides were investigated in solution with 0.001 mol/L and 0.01 mol/L cation concentration (Fig. S7a). No significant effect of the tested cations was observed at 0.001 mol/L. However, when concentration increased to 0.01 mol/L, the effect of individual cation can be seen in the order as: $Na^+ < Mg^{2+} < Co^{2+} < Ca^{2+} < K^+$ for Ba^{2+} ion and $Mg^{2+} < Co^{2+} < Na^+ < Ca^{2+} < K^+$ for Cs^+ ion (Fig. S7b). This study reveals that K^+ ion more competing than other ions due to its size that is closely related to NH_4^+ ion, thus further supporting selective adsorption of Ba^{2+} ion.

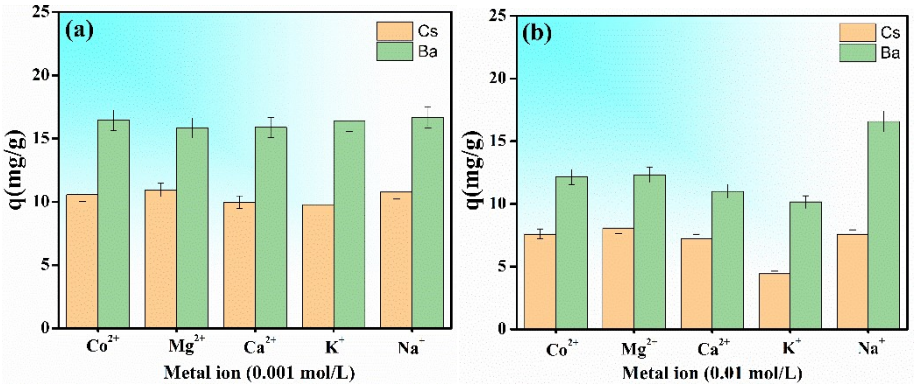

Fig. S7 Bar-graph of the

adsorption performance for Ba^{2+}/Cs^{+} ions using AW-MXene in presence of metal ions such as Co^{2+}, Mg^{2+}, Ca^{2+}, K^{+} and Na^{+} at (a) C_0 = 0.001 mol/L and (b) C_0 = 0.01 mol/L, (at pH = 5.8, m/V: 5 g/L).

References

1 S. Lagergren. Handlingar, 1898, **24**, 1-39.

2 Y. S. Ho, G. McKay, *Process Biochem.*, 1999, **34**, 451-465.

3 Y. S. Ho, G. McKay, *Process Saf. Environ. Prot.*¸ 1998, **76**, 183-191.

4 W. J. Weber and J. C. Morris, *J. Sanit. Eng. Div.*, 1963, **89**, 31-59.

5 J. Wang and X. Guo, *J. Hazard. Mater.*, 2020, **390**, 122156.

6 A. R. Khan, S. M. Husnain, F. Shahzad, S. Mujtaba-ul-Hassan, M. Mehmood, J. Ahmad, M. T. Mehran and S. Rahman, *Dalton Trans.*, 2019, **48(31)**, 11803-11812.

7 B. M. Jun, C. M. Park, J. Heo and Y. Yoon, *J. Environ. Manage.*, 2020, **256**, 109940.

8. A. K. Fard, G. Mckay, R. Chamoun, T. Rhadfi, H. Preud'Homme and M. A. Atieh, *Chem. Eng. J.*, 2017, **317**, 331-342.

9. W. Mu, S. Du, Q. Yu, X. Li, H. Wei and Y. Yang, *Dalton Trans.*, 2018, **47(25)**, 8375-8381.

10 I. Langmuir, *J. Am. Chem. Soc.*, 1918, **40**, 1361-1403.

11 H. M. F. Freundlich, *Z. Phys. Chem.*, 1906, **57A**, 385-470.

12 Q. Hu and Z. Zhang, *J. Mol. Liq.*, 2019, **277**, 646-648.

13 M. Dubinin, E. Zaverina and L. Radushkevic, *Zh. Fiz. Khim.*, 1947, **21**, 1351-1362.

14 J. Liu, D. Su, J. Yao, Y. Huang, Z. Shao and X. Chen, *J. Mater. Chem. A*, 2017, **5**, 4163-4171.

15 Y.-M. Ren, J. Yang, W.-Q. Ma, J. Ma, J. Feng and X.-L. Liu, *Water Res.*, 2014, **50**, 90-100.